La2Zr2O7 single buffer layer for YBCO RABiTS coated conductors — Source link ⎋

T. Caroff, S. Morlens, Adulfas Abrutis, Michel Decroux ...+6 more authors

Institutions: Centre national de la recherche scientifique, Vilnius University, University of Geneva

Related papers:

- Detailed investigations on La2Zr2O7 buffer layers for YBCO-coated conductors prepared by chemical solution deposition

- Growth of thick chemical solution derived pyrochlore La2Zr2O7 buffer layers for YBa2Cu3O7−x coated conductors

- Chemically deposited La2Zr2O7 buffer layers for YBCO-coated conductors : film growth and microstructure

- An all chemical solution deposition approach for the growth of highly textured CeO2 cap layers on La2Zr2O7-buffered long lengths of biaxially textured Ni–W substrates for YBCO-coated conductors

- Deposition of La2Zr2O7 film by chemical solution deposition

Share this paper: 𝑓 🐦 in ✉

La2Zr2O7 single buffer layer for YBCO RABiTS coated Conductors

Tristan Caroff, Stéphanie Morlens, Adulfas Abrutis, Michel Decroux, Patrick
Chaudouët, Laureline Porcar, Z. Saltyte, Carmen Jiménez, Philippe Odier,
François Weiss

La$_2$Zr$_2$O$_7$ single buffer layer for YBCO RABiTS coated Conductors

T. Caroff[1,2], S. Morlens[2], A. Abrutis[3], M. Decroux[4], P. Chaudouët[1], L. Porcar[2], Z. Saltyte[3], C. Jiménez[1], P. Odier[2], F Weiss[1]

1 - Laboratoire des Matériaux et du Génie Physique – CNRS UMR 5628 INPGrenoble, Minatec - 3 parvis Louis Néel - BP 257- 38016 Grenoble - France
2 - Institut Néel – CRETA CNRS UPS 2070- 25, Avenue des martyrs - BP 166 – 38042 Grenoble - France
3 - Dept of General and Inorganic Chemistry - Vilnius University - Naugarduko str.24, LT-03225 Vilnius - Lithuania.
4 - Dept of Condensed Matter Physics, University of Geneva, 24 quai Ernest Ansermet CH-1211 Geneva 4 – Switzerland

Abstract. Chemical deposition methods like MOD and MOCVD are promising approaches for coated conductors (CCs) due to their reduced cost and easy scaling. High quality La2Zr2O7 (LZO) buffer layers were prepared by MOD on Ni-5%at.W (NiW) RABiTS and subsequent YBCO layers (450 to 800 nm thick) were deposited by pulsed injection MOCVD, leading to a simple low cost architecture NiWRABiTS/LZOMOD/YBCOMOCVD. In this novel combination of MOD and MOCVD approach, a single LZOMOD buffer layer is sufficient to ensure structural compatibility between YBCO and NiW, and protect the substrate from oxidation during YBCO MOCVD. YBCO films were epitaxially grown on LZO and exhibited critical current densities Jc close to 1 MA/cm2 at 77 K with a critical temperature Tc = 91 K and ΔTc < 1 K.

1. Introduction

Chemical deposition processes have been identified as leading candidates for the development of low cost coated conductors (CCs) on rolled assisted biaxially textured substrates (RABiTS): they offer significant cost advantages compared to Pulsed Laser Deposition (PLD) processes [1-3]. Such CCs have already been developed by an all-MOD (metal organic decomposition) approach [4] which gives good results. Metal organic chemical vapor deposition (MOCVD) is another very powerful candidate for producing high quality CCs. This method is based on a ledge growth mechanism which affords an epitaxial growth. Highly textured YBCO required for high critical current CCs [5] have already been obtained that way, for example at Superpower-Inc [6]. A thick film MOCVD technology has been scaled up by this company in the Pilot MOCVD system to produce 155 meters long wire with a minimum critical current of 320 A/cm. However MOCVD is generally performed in oxygen rich atmosphere which leads to random oxidation of the metallic substrates. The solution proposed by Superpower-Inc although very performing is however a very complex combination of various processes. By our side, we are working on a simpler approach using a combination of MOD and MOCVD which is an interesting alternative to use RABiTS in CCs. The deposition and crystallization of a first buffer layer by MOD under reducing atmosphere (Ar + 5%H2) permit to avoid oxidation of the substrate during annealing. Then, if this buffer layer is an efficient barrier against oxygen diffusion, MOCVD could then be used to deposit the YBCO film. Compatibility between these two chemical deposition methods was not yet investigated; the aim of this paper is to cover this gap.

We choose pyrochlore La2Zr2O7 (LZO) as buffer layer because its lattice parameters match these of YBCO ($|(\text{YBCO- LZO})/ \text{LZO}| = 1.05$ %), and also because it provides a good barrier against O2 diffusion [7-8]. Moreover it is a highly refractory material and its recrystallization is hardly possible below 1500°C, making possible to grow more stable interfaces than with CeO2. Since this material fills all the characteristics for buffer layers (structural and chemical compatibility between substrate and active layer), a simple low cost architecture NiWRABiTS/LZOMOD/YBCOMOCVD can be achieved. To date, this concept was proved by depositing YBCO by PLD on LZOMOD [9]; in the same article YBCOMOD from TFA was also tested on LZOMOD, but an intermediate CeO2 layer was needed

to avoid reaction between LZO and YBCO films. In the present paper, we report for the first time on a single buffer layer architecture obtained by combining two chemical methods: YBCO deposited by MOCVD on NiWRABiTS substrate covered by a single LZOMOD buffer layer. The results obtained on this new low cost architecture NiWRABiTS/LZOMOD/YBCOMOCVD are presented based on data from Xray, SEM, EBSD characterizations and current transport properties.

2. Experimental

2.1 Nickel substrates

Ni-5%at.W RABiTS tape was supplied by Evico GmbH (Dresden). The RABiTS® process, described previously [10], allows to produce cheap and biaxially textured substrates. They have acute textures (in-plane FWHM = 6° 0.5°, out-of-plane FWHM = 5.5° 0.3° in the rolling direction (RD) and 9° 0.3° in the transverse direction (TD)) and a small roughness (mean square roughness rms < 5 nm). The grain size of the substrate is around 50 µm and its thickness is 150 µm.

2.2 Preparation of the LZO buffer layer Lanthanum zirconate was produced on NiW substrates by MOD according to a procedure previously described [11]. Lanthanum (III) 2,4-pentadionate and Zirconium (IV) 2,4-pentadionate were dissolved in propionic acid (CH_3-CH_2-COOOH) to form lanthanum and zirconium propionates. Solutions were stirring for 2 h at 60°C and propionic acid was added to get a concentration of 1 mol/l for total cations. LZO layers were grown on NiW substrates and on $LaAlO_3$ single crystal for comparison. Substrates were first ultrasonically cleaned in ethanol and acetone during 10 min. The films were deposited by dip coating at room temperature in a glove-box to control the hygrometry, the turbulences of air and also dust pollution, what can affect the deposition homogeneity. The substrates were immersed for 30 s in the solution and withdrawn at the speed of 2.5 cm/min. The samples were dried at 80°C under infrared lamps for 60 s inside the glove box. The films were then annealed at 960°C under a Ar + 5% H_2 gas flow with a controlled gas speed (v_{gaz} = 5.10-3 m/s) using an heating rate of 550°C.h-1 with a dwell time of 1h.

2.3 Preparation of the YBCO superconducting layer

The YBCO layer was deposited by pulsed injection MOCVD on the LZO buffered metal tape. A single liquid source based on flash evaporation using pulsed injection

CVD [12] was used to evaporate the solution. This method allows a precise control of the vapor phase composition as well as the film growth rate and the film thickness [13]. A detailed description of the PI-MOCVD reactor has already been reported elsewhere [14]. The injector sequentially delivered precise micro-doses of an organic solution containing a mixture of Y(tmhd)3, Ba(tmhd)2, Cu(tmhd)2 (tmhd = 2,2,6,6-tetramethyl-3,5- heptanedionate) dissolved in monoglyme with the appropriate molar ratio. The flash evaporation of the solution is performed at 280°C and the deposition takes place at 800°C under a controlled atmosphere (60% Ar + 40% O2) at 5 Torr. The other deposition parameters are listed in Table 1. We also deposited a CeO2 layer from a solution of Ce(tmhd)4 dissolved in monoglyme at 750°C in similar conditions to those of the YBCO layer.

2.4 Characterization techniques

The texture of the films and the epitaxial relations among the different layers were determined by X-Ray Diffraction (XRD) in Shultz geometry with a D5000 Siemens. The surface morphology was observed by Scanning Electron Microscopy (SEM) on a Philips XL30, the roughness of the films was measured by Atomic Force Microscopy (AFM) on a Veeco Dimension 3100, and the misorientations of grain boundaries of the different layers were investigated by Electron Backscattered Diffraction (EBSD) on a Zeiss ultra 500. The composition of YBCO was checked by Energy Dispersive X-ray Spectroscopy (EDS). The thickness measurements of YBCO were performed by profilometry and IRvisible reflectometry has been used to characterize the LZO thickness. The critical temperature measurements (Tc) were performed by AC-susceptibility method and the critical current density (Jc) was measured at 77 K by the 3rd harmonic measurement method [15]. In this method the critical current density is calculated from the non linear response of the third harmonic caused by the dissipation of the superconducting currents induced by a sinusoidal magnetic field. A voltage appears at the 3rd harmonic in the signal of the exciting magnet when the current is dissipated in the film. The magnetic field value B// obtained at the transition is correlated to Jc, Equation 1, where B// is the parallel component of the magnetic field with respect to the superconducting film normal, e the thickness of the film, μo the vacuum magnetic permeability and λ the London length penetration of the superconducting material.

$$J_c = \frac{B_{ll}}{\mu_0 \lambda \tanh\left[\frac{e}{\lambda}\right]} \xrightarrow{e \ll \lambda} \frac{B_{ll}}{\mu_0 \lambda} \qquad\qquad (1)$$

For films with thicknesses (e) larger than   the evaluation of Jc can be achieved only with the full equation and therefore we have assumed that the London penetration depth of our films is the one reported for good thin films (λc-YBCO = 150 nm). The measures obtained were compared with DC-fourterminals- probe measurements with the criterion of 1 µV/cm. A silver shunt was deposited ex-situ by thermal vacuum deposition, followed by a thermal treatment under O2 at 500°C, to ensure a good current transmission to the superconducting layer during Jc DC-four terminal measurements.

3. Results and discussions

3.1 LZO buffer layer

The choice of LZO as buffer layer for YBCO coated conductor lays on its behavior as diffusion barrier against oxygen, besides the crystallographic matching. The crystal structure of LZO is cubic pyrochlore with a lattice parameter a = 10.79 Å, and presents a very small lattice mismatch with YBCO (1.05%). Nevertheless, the key factor to ensure an epitaxial growth of the YBCO layer is the surface crystallinity of the LZO layers. From this point of view, the texture of the layer has to be quantified in the volume by X-ray diffraction (XRD) analyses, but also by surface sensitive techniques like EBSD (depth probed ~10 nm).

We have deposited LZO on NiW substrates and on LAO single crystals by dip-coating. According to recent searches [16-17], 80 nm of LZO is thick enough to ensure a good barrier against oxygen diffusion. The withdrawal speed was varied to obtain different film thicknesses. The thickness of our layers was determined by IR-visible reflectometry and the deposition conditions were optimized for a value of 80-100 nm. In these conditions the layers were crack-free.

The texture quality of the LZO layer was quantified by XRD. The out-of-plane orientation ωFWHM was determined from ω-scans of (004) peaks for both longitudinal (RD) and transverse (TD) direction with respect to the rolling direction of NiW, and the in-plane orientation φFWHM was determined from φ-scans of the (222) peak. The LZO out-of-plane orientation ωFWHM was around 5.3° ± 0.2° in the rolling

direction, 8° ± 0.3° in the transverse direction and the in-plane texture φFWHM was 7° ± 0.3°.

These values are summarized in Table 2. This study confirmed that most of the LZO grains had a (001) orientation (no peaks from other orientations are present in the θ-2θ diffractogramm) and confirmed that LZO film nucleates with a biaxial texture over the substrate with its unit cell axis rotated by 45° with respect to the substrate, figure 1. The texture of the LZO layer was strongly improved when deposited on LAO: in-plane φFWHM = 1° and out-of-plane ωFWHM = 0.7°. These results show that the LZO crystallographic texture is mainly dependent of the substrate quality, and show in the same time that LZO texture is as good as the one of the corresponding substrate. Two phases of LZO have been observed: fluorite or pyrochlore. Pyrochlore structure (S.G.: Fd- 3m) is derived from the fluorite structure (S.G: Fm-3m) with one-eighth of the anions absent and the other cations ordered on two cation sites. The pyrochlore structure is more efficient against oxygen diffusion due to the more ordered cations structure [7]. We have determined the presence of the pyrochlore phase in our LZO samples by X-ray diffraction using (111) and (331) reflections, corresponding to a spacing value of 6.24 Å and 2.48 Å respectively, which do not exist in the fluorite structure. The (111)-φ scan recorded at 2θ = 14.2°, χ = 54.7° revealed four reflections and the (331)-φ scan recorded at 2θ = 36.23°, χ = 46.5° revealed eight reflections as expected for the Fd-3m pyrochlore structure [18], figure 2. The presence of these two reflections proved the presence of pyrochlore structure, but not necessarily in the entire volume: a co-existence of the both structures is still possible and was admitted in a previous work [8].

The investigation of the LZO surface microstructure was performed by AFM. The picture obtained, figure 3, showed a homogeneous grain distribution with an average grain size close to 30-50 nm. The mean square roughness (rms) of the LZO layer is very small, 1.1 nm. These values are even smaller than those found by S. Sathyamurthy (5.4 nm [9]) for samples treated at 1100°C, but also smaller than those found by Knoth (~3 nm [8]) for the same annealing temperature. A smooth surface is mandatory to obtain a good interface with the superconducting layer.

The surface crystallinity was studied by EBSD as this technique probes the first 10 nm of the samples. We studied the quality of the texture at the surface of the different layers for each step. The figure 4 shows a comparison of three surfaces: NiWRABiTS

(4.a), LZO layer on NiW (4.b) and YBCO layer on NiW/LZO (4.c). The images were not taken at the same location, but are representative of the whole sample. The triangles represent the inverted pole figures showing the three main orientations of the crystallites displayed in three different color gradients in the EBSD map. The desired orientation <001> was arbitrary represented in blue. The color gradient represents out-of-plane disorientation angle of a specific grain with respect to the normal of the sample [001]. Most of the LZO grains have a <001> orientation: the fraction of the <001> oriented grains (in blue gradient) with a maximum disorientation angle of 15° is 99% for Ni and 99.5% for LZO for the same scanning size. Some disoriented grains are detected at the LZO or NiW surface, but are exceptionnaly few. In order to visualize the percolation way among the grains, we have studied the distribution of the grain boundaries angles measured by EBSD. We have chosen three windows corresponding to critical values: up to 7° (in green), from 7° to 10° (in purple), and over 10° (in red). Figure 5 shows a comparison of NiW and NiW/LZO grain boundaries. It is easy to notice that LZO reproduces the NiW microstructure. The grain structure of the NiW substrate is transferred to the buffer layer (figure 4.a,b and 5.a,b): LZO growth is templated by the orientation of NiW grains, following [001] direction (figure 6). The EBSD grain boundary maps (figure 5) show that the intergrain misorientations are smaller in the LZO film than in the NiW substrate: 53% of the grain boundaries have a misorientation angle smaller than 7° for LZO layer, against 68% for the substrate (figure 5 in green). This seems to be due to a step-mismatch mechanism, described previously by Budai et al. [19], which happens at high temperature. It is controlled by the local surface miscut angle ( ) of NiW grains which introduces a tilt angle ($\Delta\alpha$) between substrate and buffer growth direction (figure 6). This induces a relaxation of the LZO grains which reduces intergrain misorientation angle compared to the substrate which is confirmed by out-of-plane XRD texture measurements (see table 2). This enhances the texture quality and allows better percolation paths in the YBCO film. This study confirmed the quality of the texture at the surface of the different layers.

3.2 Growth of YBCO on LZO buffered tape

The performance of the LZO buffer layers was evaluated by depositing YBCO by MOCVD on these films. 450 to 800 nm thick YBCO layers were deposited on NiW/LZO by MOCVD. No NiO was produced during YBCOMOCVD depositions as confirmed by the absence of any NiO peak in the X-ray study of the heterostructure,

figure 7. This confirmed our expecting results and the previous results: 80-100 nm thick LZO layer is enough to ensure a good protection against oxygen diffusion. There is mainly no interaction between NiW and LZO layers and only pure and well oriented YBCO has grown over the LZO film: only NiW(j00), LZO(j00) and YBCO(00l) peaks are visible in the θ-2θ diffractogramm, figure 7. However, a limited interaction between the LZO and YBCO films can be detected by XRD: the presence of a small BaZrO3 (BZO) layer was detected by a φ-scan of the (110) BZO plane at $2\theta= 28.8°$ and $\chi= 45°$.

The texture of YBCO layer has also been quantified by X-Ray diffraction. The out-of-plane orientation ωFWHM was determined from ω-scans of (005) peaks for RD and TD, and the in-plane orientation φFWHM was determined from φ-scans of the (103) peak. The YBCO out-of-plane alignment with respect to the substrate is improved whereas the in-plane alignment decreases: the ωRD-FWHM decreases from 5.3° ±0.3° for the LZO films to 5.2°±0.3° for the YBCO layers in the rolling direction, and the φFWHM increases from 7° ± 0.3° for LZO to 7.5° ± 0.3° for YBCO, table 2. These values are good enough to ensure a good percolation of the current [20]. An X-ray diffraction study showed a good epitaxial growth of the YBCO layer on the LZO buffer layer, what is confirmed by EBSD. The EBSD mapping of YBCO layer (figure 4.c) was performed on a smaller scanning surface to obtain a good measurement configuration and no post-manipulation was done to erase potential unsolved Kikuchi patterns. The EBSD study proved that the YBCO layers have a good surface crystallinity on the first 10 nm and showed that most of the YBCO grains have a <001> orientation. This study indicates that the grain structure of the NiW substrate, which is transmitted to LZO layer, is also transferred to the YBCO layer. A/b-axis grains corresponding to <100> orientation are detected (0.5 - 1 μm grains, figure 4.c in red), but not in a separated grains. The c-axis proportion within a misorientation greater than 15° is around 82% of the sample surface, and the a/b-axis proportion is aroud 18%.

A SEM study showed that YBCO grown on the LZO single buffer layers had a homogeneous microstructure with 500 nm pinholes, figure 8. This is a classical morphology for YBCO films grown by MOCVD [21-22]. Pinholes and a-axis grains reduce the YBCO cross section and the critical current density as demonstrated in the heterostructures obtained by MOD [23]. The different morphologies are correlated

with the NiW grain boundaries. Some regions have more a-axis grains or pinholes than others, and show different contrasts by SEM (figure 8). Accordingly the YBCO growth seems to be influenced by the underlying NiW grains. This may be related to the inclination of the NiW grain and also to the value of the misorientation angles of grain boundaries. These grain boundaries contribute to highly decrease the superconducting properties for misorientation angles > 7° [20]. But as most of the YBCO grain boundaries are inferior to this value, the underlying NiW grain boundaries do not strongly affect the YBCO layer properties.

3.3 YBCO superconducting properties

The superconducting properties were studied on the simple heterostructure NiW/LZOMOD/YBCOMOCVD. The Tc measurements were performed by AC-susceptibility. This measurement gives information on the critical temperature but also on the intergrain coupling (correlated with ΔTc). It shows Tc close to 91 K with a sharp transition ΔTc = 0.8 K (figure 9.a): this sharp transition indicates a good oxygenation of YBCO and a good interconnectivity between YBCO grains.

Jc were measured by the 3rd harmonic measurement method. We obtained values in the range 0.5

MA/cm2 < Jc < 0.8 MA/cm2 at 77 K on 600 to 800 nm thick YBCO films (figure 9.b). We also tried to measure Jc by DC-four-terminals-probe with the criterion of 1 µV/cm. Due to the short length of our samples (15 mm) the current transfer length was too large compared with the size of the sample [24] and heat leaks were introduced by the transmission of the current in the current leads [25]. In this way, such measurement could be considered as a lower limit of the real critical current of the samples. Jc of 0.2 MA/cm2 (Ic/w = 8 A/cm) was measured for this heterostructure on a 800 nm thick YBCO layer. For the same architecture on LAO substrate, a Jc of 1.15 MA/cm2 was obtained by AC susceptibility measurements.

It is interesting to compare our values with other groups. Knoth et al [26] is working with the same precursor and studied the superconducting properties of the NiW/LZO$_{MOD}$/CeO$_{2PLD}$/YBCO$_{PL}$D structure. They deposited 200 nm of CeO$_2$ and 300 nm of YBCO by PLD at respectively 810°C and 750°C on a LZO-buffered Nickel substrate. With this structure they obtained a value of Jc = 1 MA/cm^2 on a 500 µm * 800 µm bridge. On the other hand, with another chemical approach for the deposition of LZO, ORNL studied different architectures: (1) Ni / Y$_2$O$_3$ (by e-beam) / LZO (200 nm MOD) / CeO$_2$ (60 nm MOD) / YBCO (0.8 µm TFA) with very good transport

properties (Jc = 2.5 MA/cm^2 and Ic/w= 200 A/cm), nevertheless a strong interaction among the sequential layers was detected by XRD (NiWO4, NiO, BaF$_2$, BaCeO$_3$ and poly YBCO) [26]; (2) and a single buffer layer structure [15] Ni/LZO (50 nm MOD) / YBCO (250 nm PLD) with Jc = 1.1 MA/cm^2 which decreased to Jc = 0.83 MA/cm^2 when depositing the same structure on Ni-1.7%Fe-3% W.

On the one hand our results (susceptibility measurements) on Jc are equivalent to these previous published results, on the other hand, the detailed XRD studies of the interaction between YBCO and LZO showed a very small presence of a BaZrO3 layer which could be at the origin of this low Jc values. We tried to improve the YBCO performance by adding a CeO2 cap layer grown by MOCVD. The thickness of this layer was optimized to 120 nm. The architecture NiW / LZO (80 nm MOD) / CeO$_2$ (120 nm MOCVD) / YBCO (800 nm MOCVD) was characterized by 3rd harmonic measurements and exhibited a Jc of 1.2 MA/cm^2. The Jc obtained by transport measurements was 0.7 MA/cm^2 (Ic/w = 50 A/cm), again limited by the transfer length of the current. Deposited on LAO, the Jc value was 2.5 MA/cm^2 for the same layer thickness. More investigation about the interface stability and quality should be made, in particular TEM studies are currently in preparation.

4. Conclusion

The feasibility to deposit YBCO by MOCVD directly on a LZO layer grown by MOD was demonstrated. The 80 nm thick layer of LZO deposited on NiW substrates is sufficient to protect the substrate from oxidation during the deposition of YBCO by MOCVD. This LZO layer improves the texture compared to NiW according to a mechanism that seems to apply in MOD at high temperature. Using low cost NiWRABiTS and a combination of MOD and MOCVD for YBCO coated conductors processing we succeeded to form a simple heterostructure composed of a single buffer layer and YBCO layer having a high critical current density close to 1 MA/cm2 at 77 K. This new architecture NiW$_{RABiTS}$/LZO$_{MO}$D/YBCO$_{MOCV}$D offers interesting perspectives for the development of low cost CCs.

Acknowledgements

colleagues from CRMHT for thickness measurements on LZO films and fruitful discussions with Yu Zeming and A.Guibadj.

References

[1] M.. Paranthaman, T.G. Chirayil, F.A. List, X. Cui, A.Goyal, D.F. Lee, E.D. Specht, P.M. Martin, R.K. Williams, D.M. Kroeger, J.S. Morrell, D.B. Beach, R. Feenstra, D.K. Christen, *J. Am. Ceram.Soc.* 84 (2001) 27.

[2] R.W. Schwartz, Chem. Mater. 9 (1997) 2325

[3] F.F Lange, *Science* 273 (1996) 903.

[4] M. Parans Pramanthas, S. Sathyramurthy, L. Heatherly, P.M Martin, A. Goyal, T. Kodenkandath, X. Li, C.L.H. Thieme, M.W. Rupich, *Physica C* 445-448 (2006) 529-532.

[5] S. Donet, F. Weiss, J.P Sénateur, P. Chaudouet, A. Abrutis, A. Teiserskis, Z. Saltyte, D. Selbmann, J. Eicker, O. Stadel, G. Wahl, C. Jimenez and U. Miller, *J. Phys*. IV France AA (2001), Pr11 319-323.

[6] www.superpower-inc.com

[7] J.W. SeO, J. Fompeyrine, A. Guiller, G. Norga, C. Marchiori, H. Siegwart, J.P. Locquet, *Applied Physics Letters*, vol. 83 (25), pp. 5211-5213, 2003.

[8] K. Knoth, R. Hühne, S. Oswald, L. Schultz, B. Holzapfel, *Acta Mater*, 55(2) (2006), 517-529.

[9] S.Sathyamurthy, M.Paranthaman, H.Y.Zhai, S.Kang, T.Aytug, C.Cantoni, K.J.Leonard, E.A.Payzant, H.M.Christen, A.Goyal, X. Li, *J. Mater. Res*., 19(7),2117-2123, 2004.

[10] J. L. Soubeyroux, C.E. Bruzek, A. Girard, J. L. Jorda, *IEEE Transactions on applied supercond.,* vol. 15, No. 2, pp.2687-2690, 2005.

[11] S. Morlens, Z.M. Yu, N. Marcelin, E. Jeanneau, D. Luneau, P. Odier, *Chem. Matter*, submitted.

[12] J.P. Senateur, F. Weiss, O. Thomas, R. Madar, A. Abrutis, *Patent 93/08838, PCT Fr94/00858* (1993).

[13] J.P. Sénateur, C. Dubourdieu, F. Weiss, M. Rosina, A. Abrutis, *Adv. Mater. Opt. Electron.*, vol. 10, pp.155-161, 2000.

[14] A. Abrutis, J.P. Sénateur, F. Weiss, V. Kubilius, V. Bigeltyte, Z. Saltyte, B. Vengalis, A. Jukna, *Supercond. Sci. Technol.* vol. 10, pp.959-965, 1997.

[15] Y. Mawatari, H. Yamasaki, Y. Nakagawa, *Applied Superconductivity*, 13 (2003) 3710 – 3713.

[16] S.Sathyamurthy, M.Paranthaman, H.Y.Zhai, H.M.Christen, P.M. Martin and A.Goyal, J. *Mater. Res*. 17, 2181 (2002).

[17] L. Molina, K. Knoth, S. Engel, B. Holzapfel, O. Eibl, *Supercond. Sci. Technol* 19 (2006) 1200-1208.

[18] Sleight, A.W., *Inorg. Chem.*, volume 7, page 1704 (1968).

[19] J. D. Budai, W. Yang, N. Tamura, J.S. Chung, J. Z. Tischler, B. C. Larson, G.E. Ice, C. Park, D.P. Norton, *Nature Material*, vol 2 (2003), 487-492.

[20] D. Dimos, P. Chaudhari, J. Mannhart, *Phys. Rev. B*, 41 (1990), 4038-4049.

[21] Yutaka Yoshida, Yoshiaki Ito, Hisashi Nagai, Yoshiaki Takai, Izumi Hirabayashi, Shoji Tanaka, *Pysica C* 302 (1998) 31-38.

[22] Toshio Hirai, Hisanori Yamane, *Journal of Crystal Growth*, 107 (1991) 683-691.

[23] E Bartolomé, F. Gömory, X. Granados, T. Puig, X. Obradors, *Supercond. Sci. Technol.* 20 (2007) 895-899.

[24] A. Usoskin, A. Issaev, H.C. Freyhardt, M. Leghissa, M.P. Oomen, H.W. Neumueller, *Physica C* 372-276 (2002) 857-862.

[25] M.N. Wilson, "*Superconducting Magnets*", Clarendon Press, Oxford, (10-11), 233-278.

[26] K. Knoth, R. Hühne, S.Oswald, L. Moluna, O.Eibl, L. Schultz, B. HolzapfelThin Solid Films (2007).

Table 1. PI-MOCVD deposition conditions for YBCO

T(°C) deposition/ evaporation	precursors	ratio in solution	concentration	Injection frequency / opening time	Input Gaz	Pressure
800 °C / 280 °C	$Y(tmhd)_3$ $Ba(tmhd)_2$ $Cu(tmhd)_2$	Y:Ba:Cu 1:1.9:2.1	$[Y] = 0.02$ M	2 Hz 2 ms	Ar = 840 sccm O_2 = 600 sccm	5 Torr

Table 2. FWHM values from X-ray texture measurements on the different layers of the heterostrucutres $NiW_{RABiT}/LZO_{MOD}/YBCO_{MOCVD}$ and $LAO/LZO_{MOD}/YBCO_{MOCVD}$

substrate	In-plane texture		Out-of plane texture		
	On Ni	On LAO	RD On Ni	TD On Ni	On LAO
YBCO	(103) 7.5°±0.3°	(103) 0.8°	$(005)_{RD}$ 5.2°±0.2°	$(005)_{TD}$ 7.5°±0.3°	(005) 0.45°
LZO	(222) 7°±0.3°	(222) 1°	$(004)_{RD}$ 5.3°±0.2°	$(004)_{TD}$ 8°±0.3°	(004) 0.7°
NiW	(111) 6°±0.5°	-	$(002)_{RD}$ 5.5°±0.2°	$(002)_{TD}$ 9°±0.3°	-
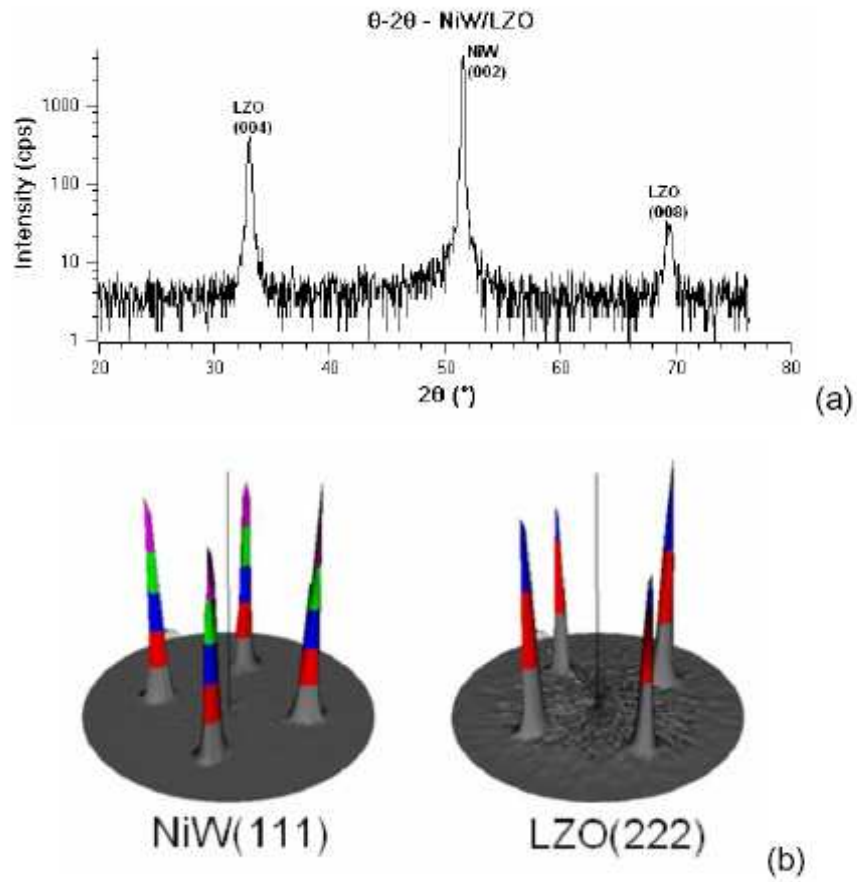
Figure 1. X-ray study of NiW/LZO: (a) θ-2θ scan - the main diffraction peaks are labelled, (b) pole figures
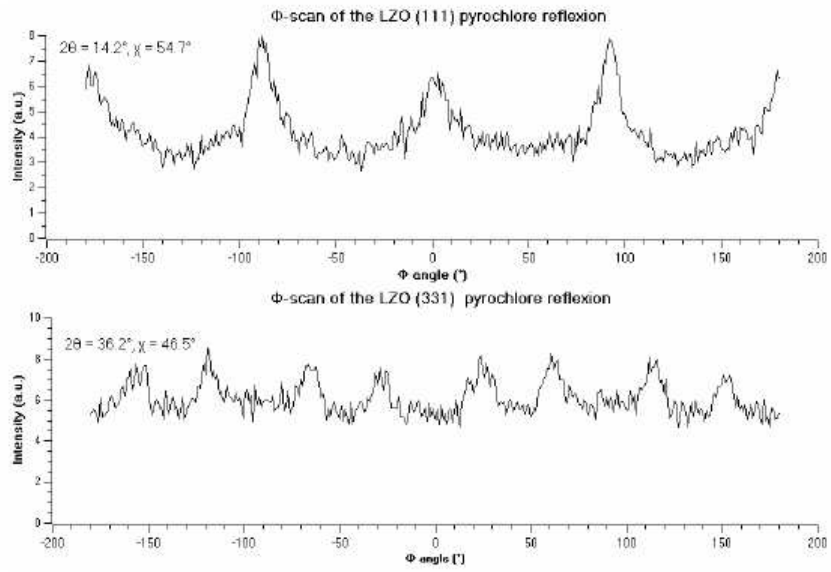
Figure 2. Φ-scan of the LZO (111) and (331) pyrochlore reflexion at respectively 2θ = 14.2°/ χ = 54.7° and 2θ = 36.2°/ χ = 46.5°
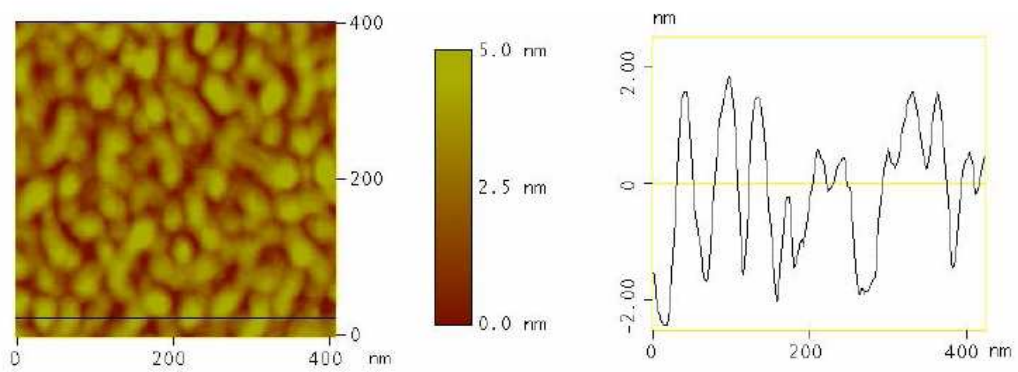

Figure 3. AFM picture of the LZO buffer layer on NiW substrate, a profile of the section is also shown. Rms roughness = 1.1 nm
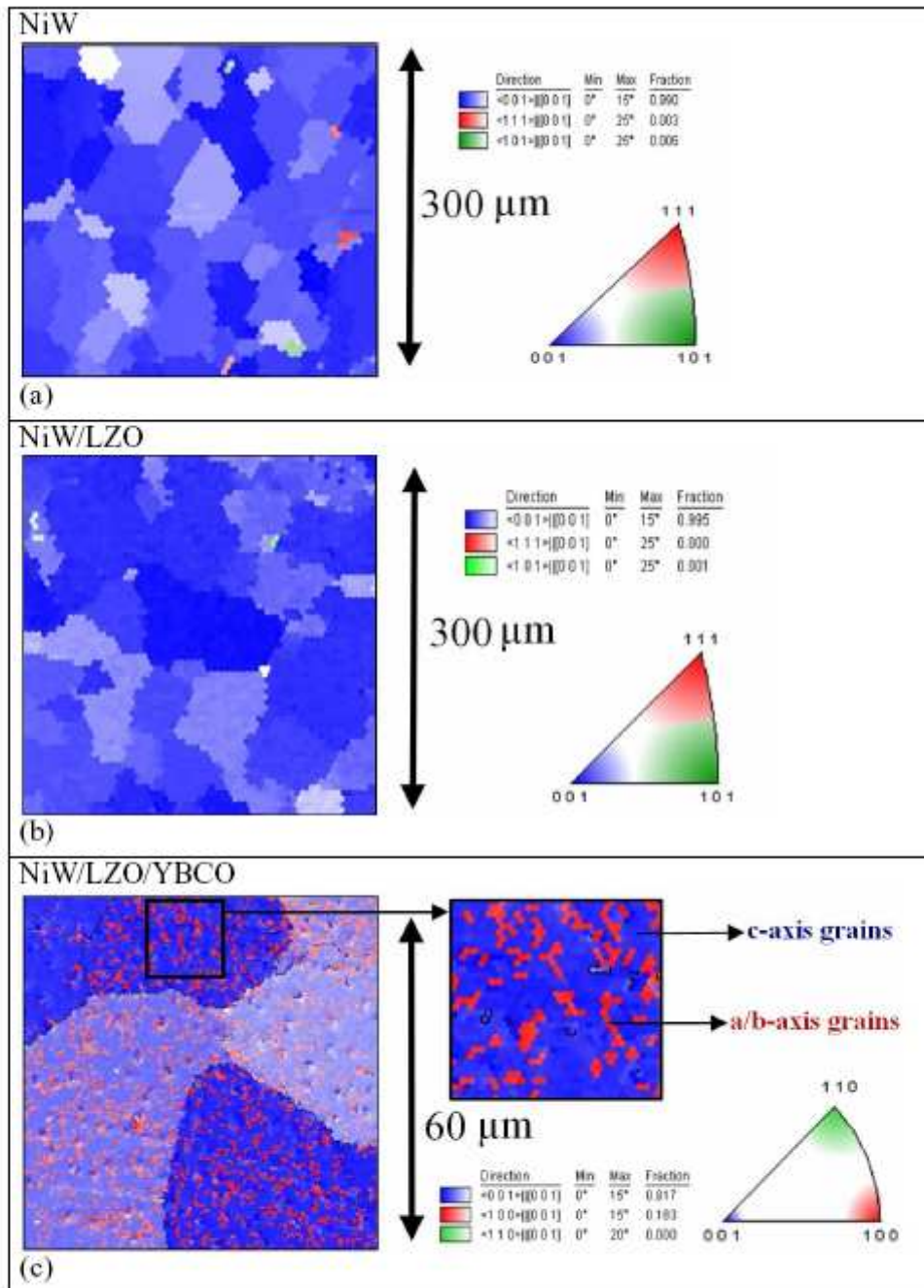
Figure 4. EBSD maps of the different layer in Ni-5%at.W$_{RABiTS}$/LZO$_{MOD}$ /YBCO$_{MOCVD}$ architecture : (a) NiW substrate, (b) NiW/LZO layer, (c) NiW/LZO/YBCO
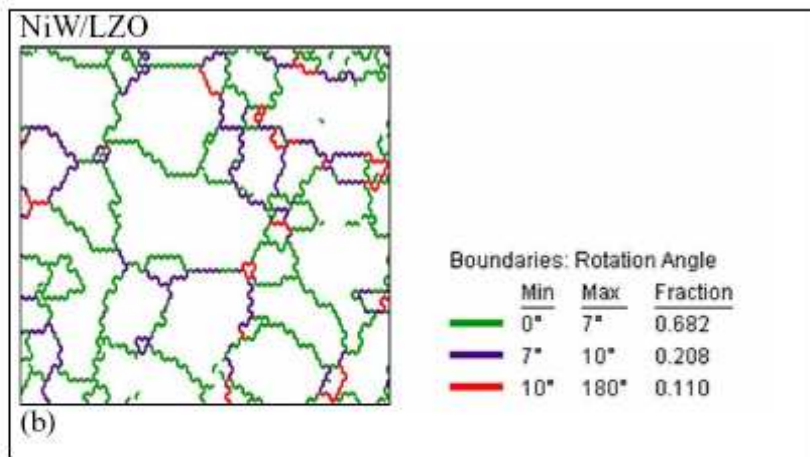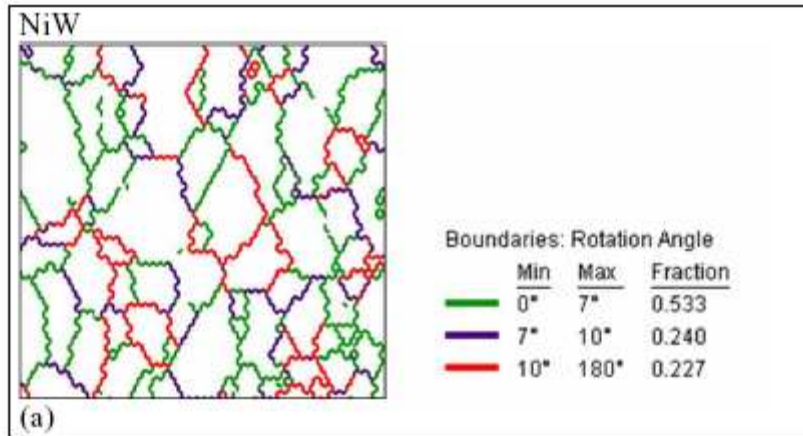
Figure 5. EBSD Grain boundaries maps of : (a) NiW substrate, (b) NiW/LZO layer from the Ni5%at.W$_{RABiTS}$/LZO$_{MOD}$
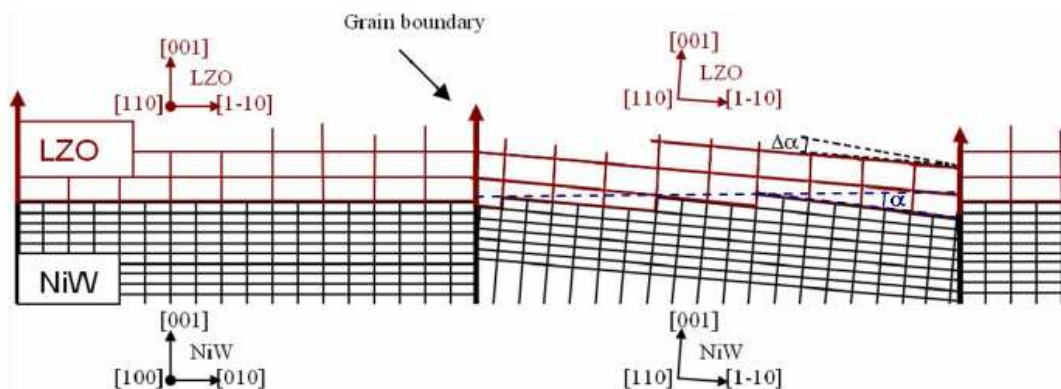

Figure 6. Growth of LZO on NiW: grain boundaries transmission. α is the local substrate surface miscut and $\Delta\alpha$ is the out-of-plane tilt angle between NiW substrate and relaxed LZO film [19].
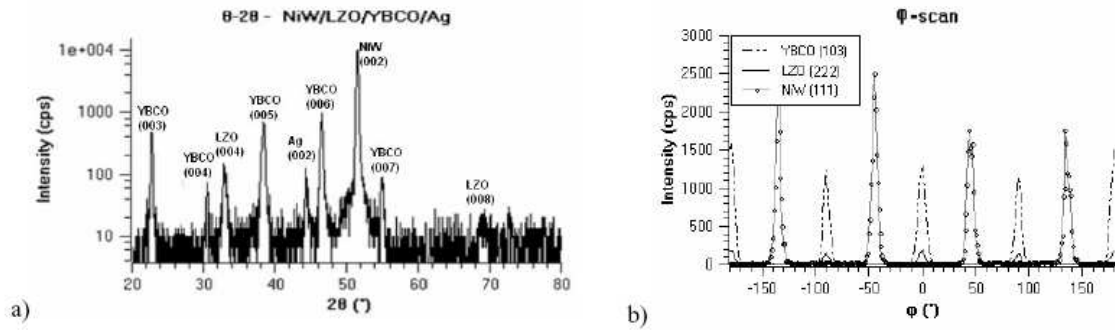
Figure 7 X-ray study of the NiW/LZO/YBCO heterostructure: (a) θ-2θ scan - the main diffraction peaks are labelled, (b) Φ-scans
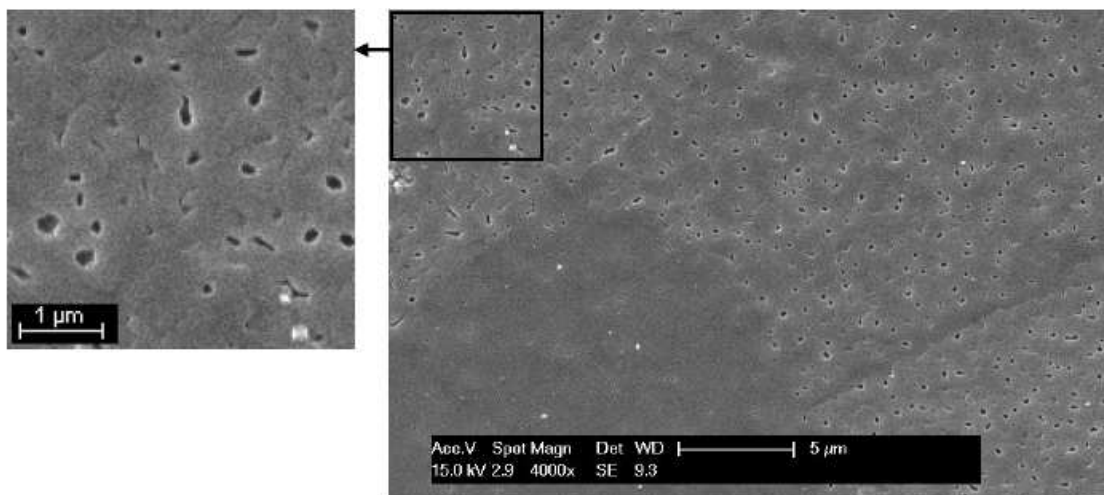

Figure 8. SEM images of the YBCO layers grown on NiW/LZO
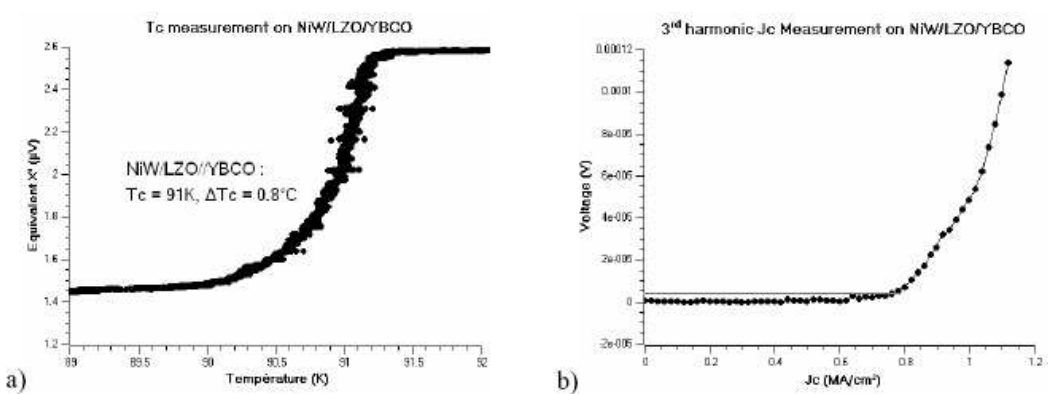

Figure 9. Superconducting properties of NiW/LZO/YBCO architecture : a) Tc by AC-susceptibility, b) Jc from 3rd harmonic at 77 K